UAV Coordination on Convex Curves in Wind: An Environmental Sampling Application

Laszlo Techy[1], Derek A. Paley[2], Craig A. Woolsey[1]

Abstract— **This paper is concerned with synchronization of UAVs, modeled as particles, moving along convex curves in the plane, in the presence of a steady wind. The method presented here integrates previous results on synchronization along convex loops, in still air, and synchronization on circles in an external flow field. The method is applied to a control-volume sampling problem, in which UAVs travel along a closed, convex curve in ambient winds in order to sample the air along a surface that bounds the control-volume. The periodic flight pattern of the UAVs is divided into a semi-circular sampling path and a near-minimum-time re-initialization path. To ensure consistent measurements, the vehicles coordinate their motion to arrive at the beginning of the sampling arcs simultaneously.**

I. Introduction

In recent years, unmanned vehicles have played an increasing role in scientific research. Autonomous underwater gliders have collected physical oceanographic measurements over unprecedented spatial and temporal scales [6], [14]. Maturing artificial intelligence techniques and improvements in automatic command and control systems allowed truly autonomous robotic mission capability on spacecraft like NASA DS1, and increased the quantity of scientific data returned from the Mars Exploration Rovers Opportunity and Spirit [1]. Unmanned aerial vehicles (UAVs) have made successful flights in Antarctica carrying miniaturized turbulence probes that measure the detailed structure of wind and temperature along the flight path [12]. The measurements can be used to estimate the heat exchange between the lower atmosphere and sea ice. UAVs have demonstrated their effectiveness in aerobiological research to monitor the movement of plant pathogens in the lower atmosphere [8]. Using autonomous vehicles as individual agents offers some advantages in addressing tasks which are "dirty, dull, or dangerous" but they provide even greater utility when networked to accomplish tasks more quickly and efficiently. Accordingly, the problem of coordinating multiple autonomous vehicles to address scientific and other missions has enjoyed increased attention from researchers.

Here we consider a specific vehicle-coordination problem: the temporal synchronization of multiple, identical flight vehicles (e.g., UAVs) along convex curves in a steady, uniform current. We assume that a suitable path has been planned, corresponding to some desired mission objective. In the application that we consider, for example, the path comprises a semi-circular arc, along which the vehicle samples the atmosphere for some constituent, and a near time-optimal arc which allows the vehicle to re-initialize for the next semicircular sampling leg. Time-optimal paths for UAVs in winds are discussed in [3], [11]. The contribution of this paper is an algorithm for coordinating the motion of multiple vehicles, modeled as constant-speed particles with steering control, along a convex path in a steady wind. A variety of coordination strategies have been proposed for such models. The papers most relevant to this work include [2] and a subsequent series of papers starting with [9], in which decentralized Lyapunov-based control laws are designed to drive a collective of vehicles to some desired, symmetric distribution along a circular orbit. The results presented in [9] are extended to motion along convex curves [5] and motion along circles in winds [4], [7]. Although we focus on the case of all-to-all communication here, the entire framework extends directly to UAV networks in which communication is time-varying and/or directed [10].

In this paper, previous results on motion coordination are extended to enable synchronization along a convex loop in the presence of a steady, uniform flow-field. A motivating application is described in which UAVs travel along convex curves designed to address an atmospheric sampling problem. Although these curves contain a zero-curvature segment, which is problematic for the proposed algorithm, we show that this segment can be replaced by a circular arc that approximates the linear segment to arbitrary precision.

The paper is organized as follows. In Section II, we describe the particle motion model and convex curves. In Section III, we describe synchronization of particle formations along closed, convex curves in the presence of a steady, uniform wind. In Section IV, we describe the control-volume sampling problem. Section V presents simulation results and Section VI summarizes and provides conclusions.

II. Modeling

A. Particle Motion in External Flow

Following previous work an control of planar formations, [4], [9], we use a particle model to describe the motion of UAVs in ambient winds. Without loss of generality we will assume that the particles are traveling at unit speed in the plane relative to a steady, uniform flow-field. To ensure forward progress of each particle in inertial space, we assume that the ambient flow speed is strictly less than one. Identifying the complex plane with the plane of motion, $\mathbb{C} \sim \mathbb{R}^2$, we express the position of each particle by the vector $r_k = x_k + iy_k$, and the flow-relative velocity of each

[1]Department of Aerospace & Ocean Engineering, Virginia Tech, Blacksburg, VA 24061 {techy, cwoolsey}@vt.edu. [2]Department of Aerospace Engineering, University of Maryland, College Park, MD 20742 dpaley@umd.edu.

particle by $e^{i\theta_k}$, where $\theta_k \in S^1$ is the orientation of the flow-relative velocity. Without loss of generality, we assume that the ambient flow is aligned with the real axis so that the equations of motion are

$$\begin{aligned} \dot{r}_k &= e^{i\theta_k} + \beta \\ \dot{\theta}_k &= u_k. \end{aligned} \tag{1}$$

Here u_k is the turn-rate control signal for the kth particle and $\beta \in \mathbb{R}$ is the external flow speed, satisfying $|\beta| < 1$.

It is convenient to express the equations in terms of the inertial speed and course angle, as opposed to the air-relative speed and heading angle. Following [4] we define the course angle as

$$\gamma_k = \arctan\left(\frac{\sin\theta_k}{\cos\theta_k + \beta}\right).$$

Using this definition one can obtain expressions for the inertial speed and course rate of change as follows [4]

$$\begin{aligned} s_k &= \beta\cos\gamma_k + \sqrt{1-\beta^2\sin^2\gamma_k} \\ \dot{\gamma}_k &= \frac{1+\beta(s_k\cos\gamma_k - \beta)}{s_k^2}\dot{\theta}_k \triangleq \nu_k. \end{aligned}$$

Then equations (1) can be written as

$$\begin{aligned} \dot{r}_k &= s_k e^{i\gamma_k} \\ \dot{\gamma}_k &= \nu_k. \end{aligned} \tag{2}$$

Equations (2) will be the model used in the following sections. Notice that, after the change in coordinates, the inertial speed of the particles is heading dependent and the new control signal is the course-rate-of-change as opposed to the heading-rate-of-change. In practice, the control u_k is calculated from ν_k. Note the mapping $\nu_k \mapsto u_k$ is invertible under the assumption $|\beta| < 1$, which implies $s_k > 0$ [4].

B. Curve Model

a) Circle: If $\nu_k = \omega_0 s_k$, $\omega_0 \neq 0$, particle k orbits a circle with radius ω_0^{-1} and fixed center

$$c_k = r_k + \omega_0^{-1} i e^{i\gamma_k}, \tag{3}$$

since, along solutions of (2),

$$\dot{c}_k = (s_k - \omega_0^{-1}\nu_k)e^{i\gamma_k} \equiv 0. \tag{4}$$

b) Convex loop: If $\nu_k = \kappa_k s_k$, where $\kappa_k = \kappa(\gamma_k) \neq 0$ is the curvature of a strictly convex loop C then particle k orbits C and the center c_k of C is fixed. Let $\rho_k = \rho(\phi(\gamma_k)) = r_k - c_k$, where $\rho : \phi \mapsto \rho(\phi)$ and $\phi : \gamma_k \mapsto \phi(\gamma_k)$ are smooth maps. If the inertial velocity of particle k is tangent to C, then [5]

$$e^{i\gamma_k} = \left|\frac{d\rho}{d\phi}\right|^{-1}\frac{d\rho}{d\phi}, \tag{5}$$

and

$$\kappa(\gamma_k) = \frac{d\gamma_k}{d\sigma}, \tag{6}$$

where

$$\sigma(\phi) = \int_0^{\phi}\left|\frac{d\rho}{d\bar{\phi}}\right| d\bar{\phi} \tag{7}$$

is arc length. Using (5)–(7), we find

$$\kappa_k^{-1} = \frac{d\sigma}{d\gamma_k} = \frac{d\sigma}{d\phi}\frac{d\phi}{d\gamma_k} = \left|\frac{d\rho}{d\phi}\right|\frac{d\phi}{d\gamma_k}, \tag{8}$$

and

$$\frac{d\rho}{d\gamma_k} = \frac{d\rho}{d\phi}\frac{d\phi}{d\gamma_k} = e^{i\gamma_k}\kappa_k^{-1}. \tag{9}$$

Therefore, along solutions of (2) with $\nu_k = \kappa_k s_k$, we have

$$\dot{c}_k = \dot{r}_k - \frac{d\rho}{d\gamma_k}\dot{\gamma}_k = (s_k - \kappa_k^{-1}\nu_k)e^{i\gamma_k} \equiv 0. \tag{10}$$

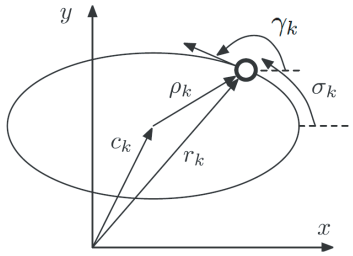

Fig. 1. The curve notation for the k^{th} particle: the position and course angle of the particle are r_k and γ_k, respectively. The curve is centered at c_k.

III. Particle Synchronization

A. Decoupled Curve Control

Lemma 3.1: For the model (2) with control input

$$\nu_k = \kappa_k s_k,$$

particle k travels along the curve C with the curve center fixed in inertial space.

The proof follows immediately from (10) (Also see [5]).

B. Translation Invariant Control

We derive decentralized control laws that drive particle k around a strictly convex loop C with a center c_0 fixed in inertial space. Define the potential function

$$S(\mathbf{r},\gamma) = \frac{1}{2}\langle \mathbf{c}, P\mathbf{c}\rangle,$$

where P is [9]

$$P = \mathrm{diag}\{\mathbf{1}\} - \frac{1}{N}\mathbf{1}\mathbf{1}^T,$$

and $\mathbf{c}$ is the vector of curve centers c_k. Note that $S(\mathbf{r},\gamma) \geq 0$ and $S(\mathbf{r},\gamma) = 0$ if and only if $\mathbf{c} = c_0\mathbf{1}$, which implies that all the curve centers coincide. The time derivative of $S(\mathbf{r},\gamma)$ along the solutions of (2) is

$$\dot{S}(\mathbf{r},\gamma) = \sum_{j=1}^{N}\langle \dot{c}_j, P_j\mathbf{c}\rangle = \sum_{j=1}^{N}\langle e^{i\gamma_j}, P_j\mathbf{c}\rangle(s_j - \kappa_j^{-1}\nu_j), \tag{11}$$

where P_j denotes the j^{th} row of P.

Lemma 3.2: The trajectories of the system (2) with the control

$$\nu_k = \kappa_k(s_k + K_0\langle e^{i\gamma_k}, P_k\mathbf{c}\rangle) \tag{12}$$

converge to a state where all particles orbit around the strictly convex curve C with a common center.

Proof: The function $S(\mathbf{r},\gamma)$ is positive definite, and its rate can be computed using (11) and control (12)

$$\dot{S}(\mathbf{r},\gamma) = -K_0 \sum_{j=1}^{N} \left\langle e^{i\gamma_j}, P_j\mathbf{c} \right\rangle^2.$$

$\dot{S}(\mathbf{r},\gamma) = 0$ if and only if

$$\left\langle e^{i\gamma_k}, P_k\mathbf{c} \right\rangle \equiv 0 \qquad k = 1,\ldots,N$$

By LaSalle's invariance principle all trajectories converge to a set Λ where $\left\langle e^{i\gamma_k}, P_k\mathbf{c} \right\rangle = 0$. In this set $\dot{\gamma}_k = \kappa_k^{-1} s_k$ and $\dot{c}_k = 0$, therefore all solutions in Λ must satisfy $P\mathbf{c} = 0$. Since the nullspace of P is the space spanned by $\mathbf{1}$ we have that in order to satisfy the invariance principle, $\mathbf{c} = c_0\mathbf{1}$, which is equivalent to the condition that the centers coincide. Application of Lemma 3.1 completes the proof. □

C. Time-splay Synchronization

In this section we extend the control law to enforce convergence to the critical set of a phase potential, such that the particles are equally separated along the curve. In [4] it is argued that the spatial separation between particles moving in external flow is not conserved in general and, instead, the temporal separation is a means for spatiotemporal regulation. Integrating the closed-loop phase dynamics

$$\dot{\gamma}_k = \kappa_k s_k, \tag{13}$$

yields

$$t = \int_0^{\gamma_k} \frac{d\gamma}{\kappa(\gamma)s(\gamma)}. \tag{14}$$

The *time-phase* is [7]

$$\psi_k = \psi(\gamma_k) = \frac{2\pi}{T} \int_0^{\gamma_k} \frac{d\gamma}{\kappa(\gamma)s(\gamma)}, \tag{15}$$

where $T > 0$ is the period of a single revolution,

$$T = \int_0^{2\pi} \frac{d\gamma}{\kappa(\gamma)s(\gamma)}. \tag{16}$$

Along solutions of (2) we have

$$\dot{\psi}_k = \frac{2\pi}{T}(\kappa_k s_k)^{-1} \nu_k. \tag{17}$$

Consider the composite potential

$$V(\mathbf{r},\gamma) = S(\mathbf{r},\gamma) + \frac{T}{2\pi} U(\psi), \tag{18}$$

where $S(\mathbf{r},\gamma) = (1/2)\langle \mathbf{c}, P\mathbf{c} \rangle$ and $U(\psi)$ is a rotationally symmetric phase potential. Rotational symmetry of U implies $\sum_{j=1}^{N} \frac{\partial U}{\partial \psi_j} = 0$. Along solutions of (2) we have

$$\begin{aligned} \dot{V} &= \sum_{j=1}^{N} \langle e^{i\gamma_j}, P_j\mathbf{c} \rangle (s_j - \kappa_j^{-1}\nu_j) + \frac{T}{2\pi}\frac{\partial U}{\partial \psi_j}\dot{\psi}_j \\ &= \sum_{j=1}^{N} \left(s_j \langle e^{i\gamma_j}, P_j\mathbf{c} \rangle - \frac{\partial U}{\partial \psi_j} \right) (1 - (\kappa_j s_j)^{-1}\nu_j). \end{aligned} \tag{19}$$

Choosing the control law

$$\nu_k = \kappa_k s_k \left(1 + K \left(s_k \langle e^{i\gamma_k}, P_k\mathbf{c} \rangle - \frac{\partial U}{\partial \psi_k} \right) \right), \; K > 0, \tag{20}$$

enforces convergence of all particles to C with a phase arrangement in the critical set of U.

Theorem 3.3: Consider the particle dynamics (2) with a smooth rotationally symmetric phase potential $U(\psi)$. The control law (20) enforces convergence of solutions to the set where all particles travel around the same convex curve, and the curve centers stay fixed in inertial space. The phase arrangement is in the critical set of $U(\psi)$.

Proof: See [9] Theorem 3.

We coordinate the time-phase on C by choosing $U(\psi)$ to be an (M,N)-pattern potential [9]. An (M,N)-pattern is a symmetric arrangement of phases consisting of M clusters uniformly spaced around the curve. In each cluster there are N/M particles. As an example $(M,N) = (2,2)$ drives two particles into two clusters that are uniformly separated along the curve. The (N,N)-pattern is the so-called splay pattern, in which the phases are uniformly separated.

IV. An Environmental Sampling Problem

In this section we give an overview of an environmental sampling problem that can be addressed using Theorem 3.3. Consider the autonomous flight of two UAVs engaged in an environmental sampling mission in which each vehicle measures some atmospheric constituent (particles, sporangia, volatile organic compounds, etc.). Suppose the area enclosed by the vehicles' flight pattern is suspected to host a source of this constituent.

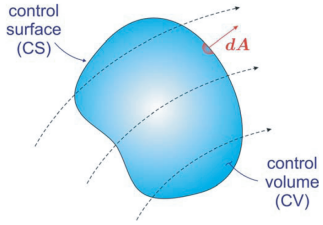

Fig. 2. Illustration of a control-volume and control surface in a flow.

Of particular interest is the control-volume sampling scenario, in which one wishes to quantify the rate of release of the measured quantity within the control-volume. The control-volume equation for the rate of change of an extensive (scalar or vector) quantity $\mathbf{Q}$ in a *fixed* volume of interest is [13]

$$\frac{d\mathbf{Q}}{dt} = \iint_{\mathrm{CS}} \frac{d\mathbf{Q}}{dm}\, \rho\, \mathbf{V}\cdot\mathbf{dA} + \frac{\partial}{\partial t} \iiint_{\mathrm{CV}} \frac{d\mathbf{Q}}{dm}\, \rho\, d\mathcal{V}$$

where $\frac{d\mathbf{Q}}{dm}$ represents the intensive value of the quantity (i.e., the quantity per unit mass) at a point in the control-volume and $\mathcal{V}$ represents volume. The total time-rate-of-change, on the left, is determined by physical principles. The first term on the right accounts for the flow of the quantity across the

control surface (the control-volume boundary) and the second term accounts for the rate of change of the property within the control-volume (see Figure 2). If $\mathbf{Q}$ represents mass, for example, the left-hand side is zero and the equation implies that the rate of increase of mass within the control-volume equals the net rate of *inflow*.

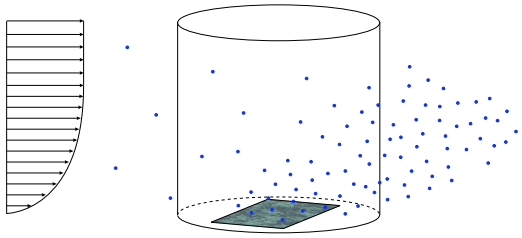

Fig. 3. Particle flow in an aerobiological sampling problem.

Suppose $\mathbf{Q}$ represents the number of particles (e.g., plant pathogen spores) in the control-volume. Suppose also that, on the spatial scale of interest, the fluid density remains constant so that $dm = \rho d\forall$. We may then write a "particle continuity equation"

$$0 = \iint_{CS} \frac{d\mathbf{Q}}{d\forall}\, \mathbf{V}\cdot\mathbf{dA} + \frac{\partial}{\partial t}\iiint_{CV} \frac{d\mathbf{Q}}{d\forall}\, d\forall.$$

The first term on the right represents the net flux of particles out of the control-volume and the second represents the rate at which particles are released within the volume (see Figure 3).

If one could measure the net outflow across the boundaries of the control-volume, that would, in turn, yield the net rate of release within the control-volume. In the framework described in this paper, the outflow across the boundaries of the control-volume is measured using two UAVs equipped with spore collection devices. The samplers may be opened in flight so that they are exposed to the incoming airflow to allow the pathogen spores to be "caught". Based on the sample time and the measured airspeed one may assess the average spore concentration. Imagine the closed flight path to be separated into two equal length portions (e.g. two halves of a circle) with an imaginary dividing line: one that lies downwind from the source and one that lies upwind from the source. The difference in the average concentration measurements along these two arcs characterizes the net outflow across the boundaries, or equivalently the net rate of spore release. If the UAVs can be equipped with multiple sampling devices that can be opened and closed in flight, then the control-volume sampling may be preformed by one vehicle that opens one set of samplers on the downwind sampling arc and another set of samplers on the upwind arc. However, if only one sampling device can be fitted onboard the UAVs, then two vehicles are necessary. The vehicles in that case modulate their sampling activity such that one of the vehicles samples upwind of the source and the other vehicle samples downwind of the source.

When the vehicles are not sampling, they re-initialize to begin the next sampling leg. Since the vehicles are not sampling during this period, they should re-initialize as quickly as possible to save time and fuel, increasing the total volume of air that is sampled. The idea is illustrated in Figure 4, where the semi-circular sampling arcs and connecting re-initialization paths are shown for both vehicles. In [11] an optimal path generation algorithm is described that generates minimum-time trajectories for vehicles flying in a constant ambient wind under turn-rate constraints. The path-generation algorithm provides a general method for constructing extremal trajectories between (sufficiently distant) initial and final points. In particular, it can be used to construct the time-optimal path from the end of the semi-circular sample leg to the beginning. We refer to the closed, convex curve that results as a "D-curve" due to its shape.

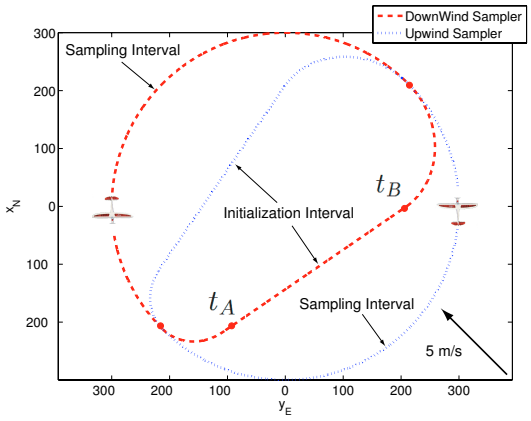

Fig. 4. Two UAVs flying in the control-volume sampling mission. UAV1 (UAV2) samples only during the upwind (downwind) path segment. The endpoints of the sampling arc are connected with a time-optimal path [11].

We note that the re-initialization interval assumes maximum control effort (maximum turn-rate), which constrains one's ability to enforce convergence to the path. In practice, the re-initialization path is generated with an artificial turn-rate limit that is strictly less than the true maximum turn-rate. This ensures that the UAV is able to track the desired path even in the presence of disturbances.

A. Parametrization of D-curves

Let $\mathbf{x}(t) \in \mathbb{R}^2$ represent a C^2 curve parameterized by the path parameter t. A C^2 curve in the plane can be uniquely described by specifying its curvature at any instant along the curve. The parametrization of the D-curves can be written as

$$\begin{aligned}
\kappa(t) &= \frac{1+\beta\,(s(t)\cos\gamma(t)-\beta)}{s(t)^3}|u_{\max}| && t\in[0,t_A]\\
\kappa(t) &= 0 && t\in[t_A,t_B]\\
\kappa(t) &= \frac{1+\beta\,(s(t)\cos\gamma(t)-\beta)}{s(t)^3}|u_{\max}| && t\in[t_B,t_C]\\
\kappa(t) &= \frac{1}{R} && t\in[t_C,T],
\end{aligned}$$

where $u_{\max}$ is the turn-rate limit used by the path generation algorithm to determine the time-optimal trajectory, and the

inertial speed $s(t)$ and course angle $\gamma(t)$ implicitly depend on the path parameter (time, in this case). In the above definition, the first and third entries correspond to the maximum turn-rate segments, the second entry corresponds to the straight segment, and the last entry corresponds to a circular segment with radius R. (Note that "turn-rate" here refers to the vehicle heading rate, which is constrained by structural limits, etc., as opposed to course rate, which depends on the ambient flow.) The first three entries correspond to the time-optimal reset path, and the last entry corresponds to the sampling interval, where the radius of curvature is held constant for the duration of a semi-circle. Notice that the time-optimal reset path has a zero curvature segment. To make the setting amenable to the synchronization algorithm described in Section III we will approximate the zero curvature segment with a circular arc of radius $R_0 \gg R$. In the limit as $R_0 \to \infty$ we obtain the straight segment.

B. Strictly Convex Approximation of the Linear Segment

Consider a smooth convex curve parameterized by t that contains a segment where the curvature is zero. To be consistent with notation in [11], let us define the path parameter where such straight segment begins by t_A and the path parameter value where it ends by t_B. Let us denote the spatial points corresponding to the these values by $\mathbf{x}(t_A)$ and $\mathbf{x}(t_B)$ and the corresponding normal vectors by $\mathbf{n}(t_A)$ and $\mathbf{n}(t_B)$ (Figure 5). Then the lines defined by the normal vectors at these points are parallel:

$$\mathbf{x}(t_A) + R_A \mathbf{n}(t_A) \parallel \mathbf{x}(t_B) + R_B \mathbf{n}(t_B), \tag{21}$$

for $R_A, R_B \in \mathbb{R}$. Moreover, as shown in the following lemma, for any specified $R_0 \in \mathbb{R}$ large enough, there exist small parameters t_A^ε and t_B^ε such that the lines normal to $\mathbf{x}(t_A - t_A^\varepsilon)$ and $\mathbf{x}(t_B + t_B^\varepsilon)$ intersect at a single point

$$\mathbf{c} = \mathbf{x}(t_A - t_A^\varepsilon) + R_0 \mathbf{n}(t_A - t_A^\varepsilon) = \mathbf{x}(t_B + t_B^\varepsilon) + R_0 \mathbf{n}(t_B + t_B^\varepsilon). \tag{22}$$

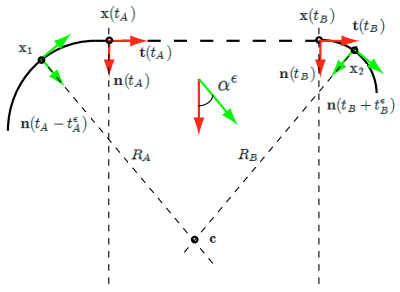

Fig. 5. Approximating the zero curvature segment with a circular arc.

Lemma 4.1: Consider a smooth, closed, convex curve $\mathbf{x}(t) \in C^2$, $t \in [t_0, t_f]$, $\mathbf{x}(t_0) = \mathbf{x}(t_f)$, $t_f = t_0 + T$ that has a zero curvature segment, where

$$\kappa(t) = 0, \qquad t \in (t_A, t_B),$$

for $t_0 < t_A < t_B < t_f$, and nonzero curvature segments, where

$$\kappa(t) \neq 0, \qquad t \in \{[t_0, t_A], [t_B, t_f]\},$$

and the curvature along the curved segments has the same sign. There exists a circle of radius R_0 that is tangent to curve $\mathbf{x}(t)$ at points $\mathbf{x}(t_A - t_A^\varepsilon)$ and at $\mathbf{x}(t_B + t_B^\varepsilon)$, for some values of $t_A^\varepsilon \in (0, t_A - t_0]$, $t_B^\varepsilon \in (0, t_f - t_B]$. The radius R_0 can be chosen arbitrarily large.

Proof: At the points $\mathbf{x}(t_A)$ and $\mathbf{x}(t_B)$ the normals are parallel by (21). Pick small $t_A^\varepsilon > 0$ (leave $t_B^\varepsilon = 0$) such that the normals intersect at point $\mathbf{c}$, and $|\mathbf{c} - \mathbf{x}(t_B)| < |\mathbf{c} - \mathbf{x}(t_A - t_A^\varepsilon)|$. Such a choice is always possible by continuity of $\mathbf{x}(t)$ and $\mathbf{n}(t)$. Now pick $t_B^\varepsilon(t_A^\varepsilon)$ such that

$$R_B(t_B^\varepsilon) = |\mathbf{c} - \mathbf{x}(t_B + t_B^\varepsilon)| \equiv |\mathbf{c} - \mathbf{x}(t_A - t_A^\varepsilon)| = R_A(t_B^\varepsilon) = R_0.$$

Then the points $\mathbf{x}(t_A - t_A^\varepsilon)$, $\mathbf{x}(t_B + t_B^\varepsilon)$ and $\mathbf{c}$ form an isosceles triangle with $\mathbf{c}$ at the corner of equilateral edges, q.e.d.

To show that such a $t_B^\varepsilon = t_B^\varepsilon(t_A^\varepsilon)$ exists, assume that it doesn't. The continuous function $f(t_B^\varepsilon) = R_A(t_B^\varepsilon) - R_B(t_B^\varepsilon) > 0$ at $t_B^\varepsilon = 0$. By convexity of $\mathbf{x}(t)$ there exists a value $t_{B\max}^\varepsilon$ where points $\mathbf{c}(t_{B\max}^\varepsilon)$ and $\mathbf{x}(t_A - t_A^\varepsilon)$ coincide, thus $f(t_{B\max}^\varepsilon) = -R_B(t_{B\max}^\varepsilon) < 0$. By continuity of $f(\cdot)$ there has to be a t_B^ε value where $f(t_B^\varepsilon) = 0$. □

In practice, one specifies a large value of the radius R_0 and executes a numerical root-finding algorithm to determine t_A^ε and the corresponding value t_B^ε (roots of equation (22)). Having done so, the definition of the D-curve becomes

$$\begin{aligned}
\kappa(t) &= \frac{1 + \beta\,(s(t)\cos\gamma(t) - \beta)}{s(t)^3}|u_{\max}| && t \in [0, t_A - t_A^\varepsilon] \\
\kappa(t) &= \frac{1}{R_0} && t \in [t_A - t_A^\varepsilon, t_B + t_B^\varepsilon] \\
\kappa(t) &= \frac{1 + \beta\,(s(t)\cos\gamma(t) - \beta)}{s(t)^3}|u_{\max}| && t \in [t_B + t_B^\varepsilon, t_C] \\
\kappa(t) &= \frac{1}{R} && t \in [t_C, T].
\end{aligned}$$

V. Simulation Results

In the previous section we described the control-volume sampling problem performed by two autonomous vehicles. In this setting the vehicles are sampling at the same altitude and ideally begin their sampling turn simultaneously. We employ a synchronization technique described in Section III to properly phase the vehicles. Notice that in the setting of Section III the vehicles share the same closed curve, and in the control-volume sampling problem the curves are different. However, due to the symmetry in the problem the time it takes for the vehicles to complete a full period is the same for the upwind sampler as for the downwind sampler (i.e. T in equation (16) is the same for both vehicles). This will ensure rotational symmetry in the time-phase (14). Initializing $t = 0$ in equation (14) for both vehicles at the instant they start their sampling interval ensures that the synchronized $(M, N) = (1, 2)$ pattern corresponds to a setting where both vehicles start and finish their sampling turn at the same time. The synchronization algorithm (20) for the model (2) has been simulated and the results can be seen in Figures 6–8. The figures show three different cases: $\beta = 0$, $\beta = 0.25$ and $\beta = 0.75$. In all three cases the two UAVs converge to equal temporal separation, and this separation is conserved during the entire loop.

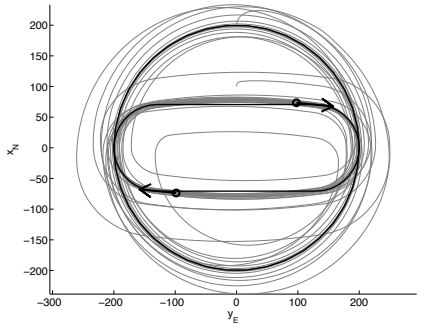

Fig. 6. Stabilization of the time-splay formation with no wind $\beta = 0$.

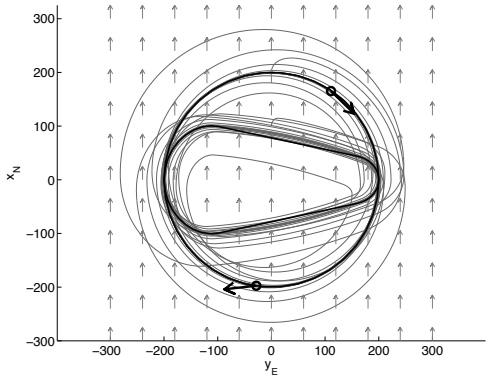

Fig. 7. Stabilization of the time-splay formation with wind speed $\beta = 0.25$ from the South.

The analysis of Section III considers unit speed particles, but the simulations presented here have been performed with dimensional parameters of a realistic aerial sampling mission. The results demonstrate that the algorithm is immediately applicable for implementation. The UAV speed has been chosen as $V_a = 20\text{m/s}$, the wind speed then is $V_w = \beta V_a$ from the South. The desired radius for the sampling mission has been chosen as $R = 200\text{m}$. The path has been designed with a maximum steady turn-rate $|u_{\max}| = 0.2832\text{rad/s}$ that comes from a technical limitation of $\phi_{\max} = 30^\circ$ on the aircraft bank angle.

VI. Conclusions

In this paper we describe a decentralized method to synchronize particle motion on general convex curves in the presence of constant ambient winds. The synchronization algorithm controls an arbitrary number of particles to a synchronized state where all particles orbit the same convex loop such that the temporal separation between them is invariant to a time shift. We described a particular application of the synchronization method for control-volume sampling using two autonomous vehicles. We show that any closed convex curve can be approximated with a strictly convex curve making the nonzero curvature assumption not restrictive for applications

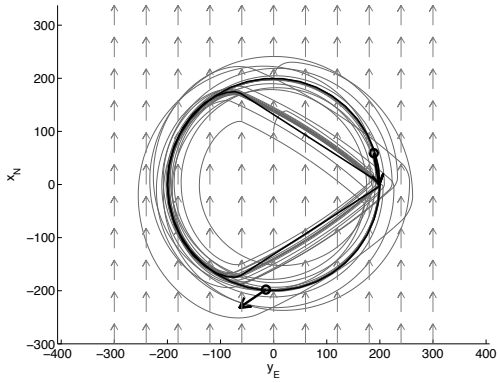

Fig. 8. Stabilization of the time-splay formation with wind speed $\beta = 0.75$ from the South.

of practical importance. We demonstrate the effectiveness of the proposed methods in simulations. Ongoing work focuses on the implementation of the described methods to be used in field experiments to monitor the spread of plant pathogen spores in the lower atmosphere.

References

[1] J. G. Bellingham and K. Rajan. Robotics in remote and hostile environments. *Science*, 318(5853):1098 – 1102, 16 November 2007.

[2] E. W. Justh and P. S. Krishnaprasad. Equilibria and steering laws for planar formations. *Systems and Control Letters*, 52:25 – 38, 2004.

[3] T. G. McGee, S. Spry, and J. K. Hedrick. Optimal path planning in a constant wind with a bounded turning rate. In *AIAA Guidance Navigation and Control Conference and Exhibit*, San Francisco, CA, August 2005.

[4] D. A. Paley. Cooperative control of an autonomous sampling network in an external flow field. In *Proceedings of the 47th IEEE Conference on Decision and Control*, Cancun, Mexico, December 2008.

[5] D. A. Paley, N. E. Leonard, and R. Sepulchre. Stabilization of symmetric formations to motion around convex loops. *Systems and Control Letters*, 57(3):209 – 215, March 2008.

[6] D. A. Paley, N. E. Leonard, R. Sepulchre, D. Grunbaum, and J. K. Parrish. Oscillator models and collective motion. *IEEE Control Systems Magazine*, 27(4):89 – 105, August 2007.

[7] D. A. Paley and C. Peterson. Stabilization of collective motion in a time-invariant flowfield. *Journal of Guidance, Control, and Dynamics*, 32(3):771 – 779, 2009.

[8] D. G. Schmale, B. R. Dingus, and C. Reinholtz. Development and application of an autonomous unmanned aerial vehicle for precise aerobiological sampling above agricultural fields. *Journal of Field Robotics*, 25(3):133 – 147, 2008.

[9] R. Sepulchre, D. A. Paley, and N. E. Leonard. Stabilization of planar collective motion: All-to-all communication. *IEEE Transactions on Automatic Control*, 52(5):811 – 824, 2007.

[10] R. Sepulchre, D. A. Paley, and N. E. Leonard. Stabilization of planar collective motion with limited communication. *IEEE Trans. Automatic Control*, 53(3):706–719, 2008.

[11] L. Techy, C. A. Woolsey, and D. G. Schmale III. Path planning for efficient UAV coordination in aerobiological sampling missions. In *Proceedings of the 47th IEEE Conference on Decision and Control*, Cancun, Mexico, December 2008.

[12] A. van den Kroonenberg, T. Spieß, and J. Bange. First wind measurements with the meteorological UAV M2AV CAROLO. *Available online: http://ams.confex.com/ams/pdfpapers/139842.pdf*.

[13] Frank M. White. *Viscous Fluid Flow*. McGraw-Hill, Inc., New York, NY, second edition, 1991.

[14] F. Zhang, D. M. Fratantoni, D. A. Paley, J. M. Lund, and N. E. Leonard. Control of coordinated patterns for ocean sampling. *International Journal of Control*, 80(7):1186 – 1199, 2007.